A PDE Approach to Coupled Super-Resolution with Non-parametric Motion

Mehran Ebrahimi and Anne L. Martel

Department of Medical Biophysics, University of Toronto
Imaging Research, Sunnybrook Health Sciences Centre
Toronto, Ontario, Canada
mehran.ebrahimi@sri.utoronto.ca, anne.martel@sri.utoronto.ca

Abstract. The problem of recovering a high-resolution image from a set of distorted (e.g., warped, blurred, noisy) and low-resolution images is known as *super-resolution*. Accurate motion estimation among the low-resolution measurements is a fundamental challenge of the super-resolution problem. Some recent promising advances in this area have been focused on coupling or combing the super-resolution reconstruction and the motion estimation. However, the existing approach is limited to parametric motion models, e.g., affine. In this paper, we shall address the coupled super-resolution problem with a *non-parametric* motion model. We address the problem in a variational formulation and propose a PDE-approach to yield a numerical scheme. In this approach, we use diffusion regularizations for both the motion and the super-resolved image. However, the approach is flexible and other suitable regularization schemes may be employed in the proposed formulation.

1 Introduction

Naturally, there is always a demand for higher quality and higher resolution images. The level of image detail is crucial for the performance of many computer vision algorithms [2,3,7,8,9,12,14,16,20].

Many of the current imaging devices typically consist of arrays of light detectors. A detector determines pixel intensity values depending upon the amount of light detected from its assigned area in the scene. The spatial resolution of images produced is proportional to the density of the detector array: the greater the number of pixels in the image, the higher the spatial resolution [16]. In many applications, however, the imaging sensors have poor resolution output. When resolution can not be improved by replacing sensors, either because of cost or hardware physical limits, one can resort to resolution enhancement algorithms. Even when superior equipment is available, such algorithms provide an inexpensive alternative. The problem of recovering a high-resolution (HR) image from a set of distorted (e.g., warped, blurred, noisy) and low-resolution (LR) images is known as *super-resolution* [2,7,8,12,14,16,20].

Fusion of the information from the observations is a fundamental challenge in the recovery process. With just one imaging device and under the same lighting conditions, we require some relative motions from frame to frame. Each LR

D. Cremers et al. (Eds.): EMMCVPR 2009, LNCS 5681, pp. 112–125, 2009.

frame should provide a different look at the same scene. Motion and nonredundant information obtained from different frames are what make super-resolution feasible [16].

1.1 A Brief History

The super-resolution literature has significantly expanded in the past 20 years. A rather recent and comprehensive survey of super-resolution techniques is given in [8]. Historically, Irani and Peleg [14] proposed an iterative back-projection method to address the super-resolution problem. Sauer and Allebach [18], and Tekalp, Ozkan and Sezan [23] modelled super-resolution as an interpolation problem with nonuniformly sampled data and used a projection onto convex sets algorithm to reconstruct the image. Ur and Gross [27] considered Papoulis' generalized multichannel sampling theorem [17] for interpolating values on a higher resolution grid. Shekarforoush and Chellappa [22] extended Papoulis' theorem for merging the nonuniform samples of multiple channels into HR data. Aizawa et al. [1] also modelled super-resolution as an interpolation problem with nonuniform sampling and used a formula related to Shannon's sampling theorem [21] to estimate values on a HR grid. Tsai and Huang [26] were among the first to superresolve a HR image from several sampled LR frames. Hardie et al. [12] proposed a joint MAP registration and restoration algorithm using a *Gibbs image prior*. Schultz and Stevenson [20] used a Markov random field model with Gibbs prior to better represent image discontinuities, such as transitions across sharp edges. More recently Farsiu et al. [9] proposed an alternative data fidelity, or regularization term based on the ℓ^1 norm which has been shown to be robust to data outliers. They proposed a novel regularization term called Bilateral-TV which provides robust performance while preserving the edge content common to real image sequences.

1.2 Coupled Motion Estimation

Accurate motion estimation has been a very important aspect of super-resolution schemes. In many existing super-resolution approaches, the motion is computed directly from the LR frames, while many other super-resolution algorithms unrealistically assume that motion parameters are precisely known. In general, however, accurate motion estimation of subpixel accuracy remains a fundamental challenge in super-resolution reconstruction algorithms.

In a recent work [6], it has been suggested that the motion can be relaxed from a strict grid mapping to a multi-pixel-pair intensity relation. In this view, pixel-pairs in different frames may be relevant to each other with some measured probability of confidence. In the method proposed in [6], instead of estimating the motion vectors explicitly, a framework is provided in which such confidence measures are evaluated and employed in the HR image reconstruction. However, the algorithm is computationally intensive.

In general, it is believed that a combined super-resolution reconstruction and motion estimation may be the key to address the super-resolution problem.

A novel method towards this direction is proposed in [4]. Although the authors of [4] appreciate the importance of considering non-parametric motion models, their proposed method is restricted to the parametric affine motion model. The fact that authors of [4] have preferred to work with a parametric motion model rather than a non-parametric one can be associated to the complexity of formulations of the non-parametric approaches as discussed in [4].

1.3 The Agenda

In this work, we propose the coupled multi-frame super-resolution problem with a *non-parametric* motion model. In Section 2, we will introduce the problem as a minimization and present its corresponding variational formulation. For consistency, we adopt our notations from [15]. In Section 3, we derive a PDE with a steady-state solution that corresponds to the solution of the described problem. The discretization and derivation of a numerical scheme for the PDE is followed in Section 4. Finally, we will present various computational experiments and concluding remarks in Sections 5 and 6.

2 Mathematical Formulation

Throughout, images are d-dimensional and are assumed as compactly supported elements of $\mathcal{L}^2(\Omega)$, $\Omega \subset \mathbb{R}^d$, unless otherwise stated.

Forward Model. Assume that m low-resolution measurement images y_1, $y_2, \dots y_m$ of an ideal image f are given. For every $i = 1, \dots, m$, y_i is a noisy, low-resolution realization of deformed copies of f via a d-dimensional vector field $u_i = (u_{i,1}, \dots, u_{i,d})$. Namely,

$$y_i := \mathcal{H} f_{u_i} + n_i, \quad i = 1, \dots, m, \tag{1}$$

where n_i is the additive noise, and f_{u_i} denotes the deformed image f via u_i, i.e., $f_{u_i}(x) = f(x - u_i(x))$. Throughout, we may also use the alternative notation of

$$\mathcal{S}_i f := f_{u_i}.$$

Note that the operator $\mathcal{S}_i$ is linear with respect to f although f_{u_i} is a nonlinear expression with respect to u_i. The operator $\mathcal{H} : \mathcal{L}^2(\Omega) \to \mathcal{L}^2(\Omega)$ is assumed to be a known linear degradation operator modeled as a composition of a spatially invariant blur $\mathcal{K}$ followed by a down-sampling operator $\mathcal{D}$, i.e., $\mathcal{H} := \mathcal{D} \circ \mathcal{K}$. Here, $\mathcal{D}$ is an impulse train constructed using the sum of uniformly spaced Dirac functions [16,8,9,3,7]. To proceed, we formulate the corresponding super-resolution problem. As opposed to what is typically common in the literature, we assume that both the deformations and the high-resolution image are unknown and try to recover both simultaneously.

Problem 1. *Given a set of m low-resolution measured images represented by $y := \{y_1, y_2, \dots y_m\}$ and a degradation operator $\mathcal{H}$, find a corresponding set of deformations $u := \{u_1, u_2, \dots, u_m\}$ and a high-resolution image f that minimizes*

$$\mathcal{J}[u, f] := \mathcal{C}[y; (u, f)] + \mathcal{R}[u, f]$$

in which $\mathcal{C}$ measures the consistency of the measurements y with the high-resolution image f, and $\mathcal{R}$ is a regularization expression on $[u, f]$. Here, we use the sum of squares of intensity differences for the consistency measure

$$\mathcal{C}[y; (u, f)] := \frac{1}{2} \sum_{i=1}^{m} ||y_i - \mathcal{H} f_{u_i}||^2_{\mathcal{L}^2(\Omega)}, \tag{2}$$

and the regularization is defined by

$$\mathcal{R}[u, f] := \sum_{i=1}^{m} \alpha_i \mathcal{P}[u_i] + \beta \mathcal{Q}[f], \tag{3}$$

in which $\alpha_1, \dots, \alpha_m, \beta \in \mathbb{R}^+$ are positive regularizing parameters. Hence, the objective is to minimize

$$\mathcal{J}[u, f] = \frac{1}{2} \sum_{i=1}^{m} ||y_i - \mathcal{H} f_{u_i}||^2_{\mathcal{L}^2(\Omega)} + \sum_{i=1}^{m} \alpha_i \mathcal{P}[u_i] + \beta \mathcal{Q}[f]. \tag{4}$$

We shall present a mathematical formulation to solve Problem 1. Briefly speaking, we seek necessary conditions for optimality of $[u, f]$ by finding the Gâteaux derivatives of the components of $\mathcal{J}$ with respect to $[u, f]$. This shall provide us with the corresponding Euler-Lagrange equations that will be used to form a PDE which will be solved numerically.

Theorem 1. *Let $d \in \mathbb{N}$, and $f, y_1, y_2, \dots y_m$ are d-dimensional real-valued images, i.e., functions from $\Omega \subset \mathbb{R}^d \to \mathbb{R}$, $f \in C^2(\mathbb{R}^d)$, $u_1, \dots, u_m : \mathbb{R}^d \to \mathbb{R}^d$, $v : \mathbb{R}^d \to \mathbb{R}^{md+1}$, $\Omega :=]0, n[^d$. The Gâteaux derivative of $\mathcal{C}[y; (u, f)]$ is given by*

$$d\mathcal{C}[y; (u, f); v] = -\int_{\Omega} \langle \Phi(x, u(x), f(x)), v(x) \rangle_{\mathbb{R}^{md+1}} \, dx,$$

in which $\Phi : \mathbb{R}^d \times \mathbb{R}^{md} \times \mathbb{R} \to \mathbb{R}^{md+1}$,

$$\Phi(x, u(x), f(x)) = [p_1(x), \dots, p_m(x), q(x)],$$

where

$$p_i(x) := \mathcal{H}^*[\mathcal{H}\mathcal{S}_i f(x) - y_i(x)] \nabla \mathcal{S}_i f(x), \quad i = 1, \dots, m,$$
$$q(x) := -\sum_{i=1}^{m} \mathcal{S}_i^* \mathcal{H}^*[\mathcal{H}\mathcal{S}_i f(x) - y_i(x)],$$

in which $\mathcal{H}^*$ and $\mathcal{S}_i^*$ represent the adjoint of operators $\mathcal{H}$ and $\mathcal{S}_i$ respectively. [see the proof in Appendix 1. Cf. [15] pp. 80.]

Here, we focus on the special case where $\mathcal{P}$ and $\mathcal{Q}$ are diffusion regularization expressions [15,11,10,13,24,25].

Theorem 2. *Assume $\mathcal{P}$ and $\mathcal{Q}$ are diffusion regularization expressions and the functionals $\mathcal{P}_i^e$ and $\mathcal{Q}^e$ are respectively trivial extensions of $\mathcal{P}$ and $\mathcal{Q}$, i.e.,*

$$\mathcal{P}_i^e[(u,f)] := \mathcal{P}[u_i] := \frac{1}{2}\sum_{j=1}^{d}\int_\Omega \langle \nabla u_{i,j}\ , \nabla u_{i,j}\rangle\ dx, \quad i=1,\dots,m, \tag{5}$$

$$\mathcal{Q}^e[(u,f)] := \mathcal{Q}[f] := \frac{1}{2}\int_\Omega \langle \nabla f, \nabla f\rangle\ dx. \tag{6}$$

Also, assume that Neumann boundary conditions are imposed, i.e.,

$$\langle \nabla f(x), \overrightarrow{n}(x)\rangle_{\mathbb{R}^d} = \langle \nabla u_{i,j}(x), \overrightarrow{n}(x)\rangle_{\mathbb{R}^d} = 0 \quad \textit{for} \quad x\in\partial\Omega \ \textit{and} \quad j=1,\dots,d,$$

in which $\overrightarrow{n}$ denotes the outer normal unit vector of $\partial\Omega$ (boundary of Ω). The Gâteaux derivative of $\mathcal{P}_i^e[(u,f);v]$ and $\mathcal{Q}^e[(u,f);v]$ are respectively

$$d\mathcal{P}_i^e[(u,f);v] = -\int_\Omega \langle \mathcal{A}_i[u](x), v(x)\rangle_{\mathbb{R}^{d+1}}\ dx, \quad i=1,\dots,m,$$

$$d\mathcal{Q}^e[(u,f);v] = -\int_\Omega \langle \mathcal{B}[f](x), v(x)\rangle_{\mathbb{R}^{d+1}}\ dx$$

where,

$$\begin{aligned}\mathcal{A}_i[u](x) &= (\underbrace{0_{\mathbb{R}^d},\dots,0_{\mathbb{R}^d}}_{i-1\ times}, \Delta u_{i,1}(x),\dots,\Delta u_{i,d}(x), \underbrace{0_{\mathbb{R}^d},\dots,0_{\mathbb{R}^d}}_{m-i\ times}, 0)\\ &= (\underbrace{0_{\mathbb{R}^d},\dots,0_{\mathbb{R}^d}}_{i-1\ times}, \Delta u_i(x), \underbrace{0_{\mathbb{R}^d},\dots,0_{\mathbb{R}^d}}_{m-i\ times}, 0),\end{aligned}$$

$$\mathcal{B}[f](x) = (\underbrace{0_{\mathbb{R}^d},\dots,0_{\mathbb{R}^d}}_{m\ times}, \Delta f(x)) = (0_{\mathbb{R}^{md}}, \Delta f(x)).$$

Proof. The result yields applying the Green's formula similar to [15] pp. 138.

Theorem 3. *The Euler-Lagrange equations corresponding to the objective expression $\mathcal{J} = \mathcal{C} + \sum_{i=1}^m \alpha_i\mathcal{P}_i^e + \beta\mathcal{Q}^e$ identical to Equation (4) where $\mathcal{C}$ is defined by Equation (2) and $\mathcal{P}_i^e$, $\mathcal{Q}^e$ are defined by Equations (5,6) respectively are*

$$\Phi(x,u(x),f(x)) + \sum_{i=1}^{m}\alpha_i\mathcal{A}_i[u](x) + \beta\mathcal{B}[f](x) = 0, \qquad x\in\Omega, \tag{7}$$

with Neumann boundary conditions. These can also be written as

$$\mathcal{H}^*[\mathcal{H}\mathcal{S}_i f(x) - y_i(x)]\nabla\mathcal{S}_i f(x) + \alpha_i\Delta u_i(x) = 0_{\mathbb{R}^d},$$

$$i=1,\dots,m, \quad x\in\Omega,$$

$$-\sum_{i=1}^{m} \mathcal{S}_i^* \mathcal{H}^* [\mathcal{H}\mathcal{S}_i f(x) - y_i(x)] + \beta \Delta f(x) = 0, \qquad x \in \Omega,$$

$$\langle \nabla f(x), \overrightarrow{n}(x) \rangle_{\mathbb{R}^d} = \langle \nabla u_{i,j}(x), \overrightarrow{n}(x) \rangle_{\mathbb{R}^d} = 0,$$

$$j = 1, \ldots, d, \quad i = 1, \ldots, m, \quad x \in \partial\Omega.$$

Proof. The result yields from Theorem 1 and substitution (Cf. [15] pp. 138.) .

3 A Corresponding PDE

There exist various ways to solve Equation (7). A possibility that we pursue here is to formulate the solution as the steady-state solution of a corresponding PDE similar to [15]. We propose

$$\partial_t (u(x,t), s\ f(x,t)) = \Phi(x, u(x,t), f(x,t)) + \sum_{i=1}^{m} \alpha_i \mathcal{A}_i[u](x) + \beta \mathcal{B}[f](x) \quad x \in \Omega, \quad t \geq 0,$$

where s is a scale factor. Assuming $\Phi = (p_1, \ldots, p_m, q)$ the PDE can be written as

$$\partial_t u^{(i)}(x,t) = p_i(x, u(x,t), f(x,t)) + \alpha_i \Delta u_i(x,t), \tag{8}$$

$$i = 1 \ldots, m, \quad x \in \Omega, \quad t \geq 0,$$

$$s\ \partial_t f(x,t) = q(x, u(x,t), f(x,t)) + \beta \Delta f(x,t), \qquad x \in \Omega, \quad t \geq 0, \tag{9}$$

where,

$$p_i(x,u,f) := \mathcal{H}^*[\mathcal{H}\mathcal{S}_i f(x) - y_i(x)] \nabla \mathcal{S}_i f(x), \qquad i = 1 \ldots, m,$$

$$q(x,u,f) := -\sum_{i=1}^{m} \mathcal{S}_i^* \mathcal{H}^* [\mathcal{H}\mathcal{S}_i f(x) - y_i(x)].$$

4 Discretization and Numerical Scheme

To numerically solve the derived PDE in Equations (8,9), we evaluate expressions at discrete time variable $\{t_{k+1}\}$

$$\partial_t u_i(x, t_{k+1}) = p_i(x, u(x,t_k), f(x,t_k)) + \alpha_i \Delta u_i(x, t_{k+1}), \tag{10}$$

$$i = 1, \ldots, m, \quad x \in \Omega,$$

$$s\ \partial_t f(x, t_{k+1}) = q(x, u(x,t_{k+1}), f(x,t_{k+1})) + \beta \Delta f(x, t_{k+1}), \quad x \in \Omega. \tag{11}$$

Notice that due to the nonlinearity of p_i with respect to u_i, f is evaluated at t_k instead of t_{k+1} in Equation (10) [cf. [15] pp. 80] which translates to applying a fixed-point iteration scheme. However, q is linear with respect to f and t_{k+1} is used consistently in Equation (11). Using a spatial discretization X of Ω that includes n^d voxels (pixels) corresponding to a unit space step in every

dimension due to the definition of $\Omega :=]0, n[^d$, and a time step of τ_1, we define for $j = 1, \ldots, d$, and $k = 0, 1, 2, \ldots$

$$U_{i,j}^k(X) := u_{i,j}(X, \tau_1 k) := Discretized(u_j(x, t_k)),$$
$$F^k(X) := f(X, \tau_1 k) := Discretized(f(x, t_k)),$$
$$Y_i(X) := y_i(X) := Discretized(y_i(x)).$$

Furthermore, $\mathbf{A}U_{i,j}^k := \Delta u_{i,j}(X, \tau_1 k) := Discretized(\Delta u_{i,j}(x, t_k))$,
$$\mathbf{A}F^k := \Delta f(X, \tau_1 k) := Discretized(\Delta f(x, t_k)),$$

in which $\mathbf{A} \in \mathbb{R}^{n^d \times n^d}$ is defined such that

$$\mathbf{A}U_{i,j}^k \approx \sum_{l=1}^{d} \partial_{x_l, x_l} u_{i,j}(X, \tau_1 k) \quad \text{and} \quad \mathbf{A}F^k \approx \sum_{l=1}^{d} \partial_{x_l, x_l} f(X, \tau_1 k).$$

[See Appendix 2 for the precise definition of $\mathbf{A}$.] Also, assume that $\mathbf{H}$ is a matrix that represents $\mathcal{H}$, and its transpose $\mathbf{H}^T$ represents $\mathcal{H}^*$ in the discretization. Appendix 3 gives the precise definition of $\mathbf{H}$, which is assumed as the matrix product of the local averaging blur $\mathbf{K}$ by a zooming factor of $z \in \mathbb{N}$ in every direction, multiplied by down-sampling matrix of factor z in every direction represented by $\mathbf{D}$. Furthermore, $\mathbf{S}_i^k$ is the sparse matrix constructed using U_i^k. This matrix provides a discrete approximation of the operator $\mathcal{S}_i$ for $i = 1, \ldots, m$. [See [4] Equations (3,4) for the precise construction of such matrix using linear interpolation for 2-dimensional images i.e., $d = 2$.]

Substituting the discretization in the PDEs of Equations (10,11) leads that for $j = 1, \ldots, d,\ k = 0, 1, 2, \ldots$

$$\frac{U_{i,j}^{k+1} - U_{i,j}^k}{\tau_1} = \mathbf{H}^T[\mathbf{H}\mathbf{S}_i^k F^k - Y_i] \ \cdot \ \partial_j \mathbf{S}_i^k F^k + \alpha_i \mathbf{A} U_{i,j}^{k+1},$$
$$s\frac{F^{k+1} - F^k}{\tau_1} = -\sum_{i=1}^{m} (\mathbf{S}_i^{k+1})^T \mathbf{H}^T [\mathbf{H}\mathbf{S}_i^{k+1} F^{k+1} - Y_i] + \beta \mathbf{A} F^{k+1}.$$

Defining $\tau_2 := \tau_1 / s$ gives

$$\Big(\mathbf{I} - \tau_1 \alpha_i \mathbf{A}\Big) U_{i,j}^{k+1} = U_{i,j}^k + \tau_1 \mathbf{H}^T [\mathbf{H}\mathbf{S}_i^k F^k - Y_i] \cdot \partial_j \ \mathbf{S}_i^k F^k,$$
$$\Big(\mathbf{I} - \tau_2 \beta \mathbf{A} + \tau_2 \sum_{i=1}^{m} (\mathbf{S}_i^{k+1})^T \mathbf{H}^T \mathbf{H} \mathbf{S}_i^{k+1}\Big) F^{k+1} = F^k + \tau_2 \sum_{i=1}^{m} (\mathbf{S}_i^{k+1})^T \mathbf{H}^T Y_i,$$

where $\mathbf{I} \in \mathbb{R}^{n^d \times n^d}$ is the identity matrix.

This yields

$$U_{i,j}^{k+1} = \Big(\mathbf{I} - \tau_1 \alpha_i \mathbf{A}\Big)^{-1} \Big[U_{i,j}^k + \tau_1 \mathbf{H}^T [\mathbf{H}\mathbf{S}_i^k F^k - Y_i] \cdot \partial_j \ \mathbf{S}_i^k F^k\Big],$$

$$F^{k+1} = \Big(\mathbf{I} - \tau_2 \beta \mathbf{A} + \tau_2 \sum_{i=1}^{m} (\mathbf{S}_i^{k+1})^T \mathbf{H}^T \mathbf{H} \mathbf{S}_i^{k+1}\Big)^{-1} \Big[F^k + \tau_2 \sum_{i=1}^{m} (\mathbf{S}_i^{k+1})^T \mathbf{H}^T Y_i\Big].$$

Finally, we use the initialization vectors $F^0 = U_{i,j}^0 = 0_{\mathbb{R}^{n^d}}$, for $i = 1, \ldots, m$, $j = 1, \ldots, d$.

5 Computational Experiments

In this Section we present a few computational examples to verify the derived numerical scheme. Figures 1 and 2 show the results of evaluating the proposed super-resolution algorithm on image sequences taken from the data-set library of MDSP at U. California Santa Cruz (`http://www.soe.ucsc.edu/ milanfar/software/sr-datasets.html`).

In Figure 1, the first $m = 30$ frames, of an 8-bits text sequence, of size 48×48 is used and independent additive white Gaussian noise of standard deviation $\sigma = 5$ is added to the LR frames. The results are shown along with the parameters described in the caption of the Figure.

In Figure 2, the same kind of experiment is performed over a total of $m = 60$ frames, of an 8-bits surveillance sequence, of size 32×32 and again independent additive white Gaussian noise of standard deviation $\sigma = 5$ is added to the LR frames. The results are shown along with the parameters described in the Figure's caption.

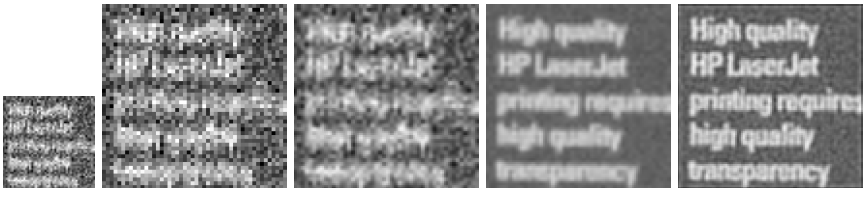

(a) (b) (c) (d) (e)

Fig. 1. (a) LR frame #1. (b) Nearest neighbor interpolation on the LR frame #1. (c) Bilinear interpolation on the LR frame #1. (d) Average of the bilinear interpolation of all 30 LR frames. (e) Super resolution result of frame #1 in $d = 2$ dimensions of $n = 48$ pixels in every dimension, zooming factor $z = 2$, total number of LR frames $m = 30$, regularization parameters α_i=4000, $i = 1, \ldots, 30$, $\beta = 1$, and time steps $\tau_1 = 0.01$, $\tau_2 = 10^{10}$, where 10 iterations are applied.

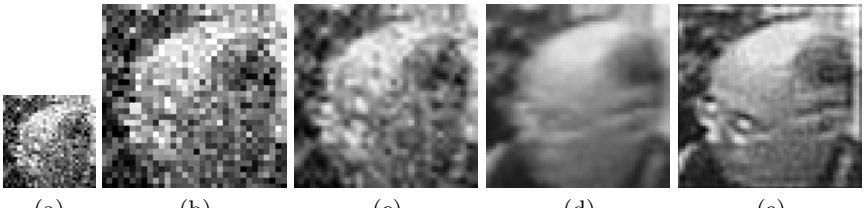

(a) (b) (c) (d) (e)

Fig. 2. (a) LR frame #1. (b) Nearest neighbor interpolation on the LR frame #1. (c) Bilinear interpolation on the LR frame #1. (d) Average of the bilinear interpolation of all 60 LR frames. (e) Super resolution result of frame #1 in $d = 2$ dimensions of $n = 32$ pixels in every dimension, zooming factor $z = 2$, total number of LR frames $m = 60$, regularization parameters α_i=4000, $i = 1, \ldots, 60$, $\beta = 1$, and time steps $\tau_1 = 0.01$, $\tau_2 = 10^{10}$, where 10 iterations are applied.

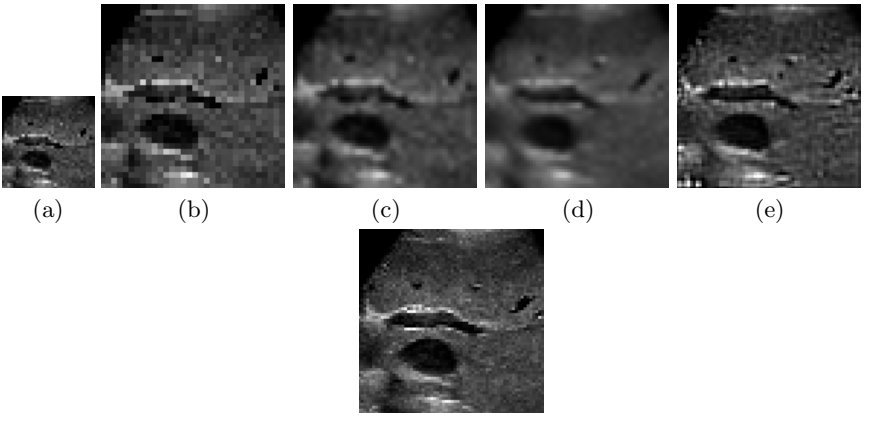

(a) (b) (c) (d) (e)

(f)

Fig. 3. (a) LR frame #1. (b) Nearest neighbor interpolation on the LR frame #1. (c) Bilinear interpolation on the LR frame #1. (d) Average of the bilinear interpolation of all 40 LR frames. (e) Super resolution result of frame #1 in $d = 2$ dimensions of $n = 32$ pixels in every dimension, zooming factor $z = 2$, total number of LR frames $m = 40$, regularization parameters α_i=4000, $i = 1, \ldots, 40$, $\beta = 0.1$, and time steps $\tau_1 = 0.01$, $\tau_2 = 10^{10}$, where 10 iterations are applied. (f) The HR ground truth relating to frame #1.

Finally, in Figure 3, we have performed the experiments over a portion of a locally-averaged and down-sampled ultrasound sequence of $m = 60$ frames of size 32×32, for which the original HR image relating to frame #1 is given in Figure 3(f). The efficiency of the technique can be simply observed by comparing the image (e) of each Figure to the other images in the figure.

Note that in all of the experiments, we have assumed $\tau_2 = 10^{10}$. In general, if we assume $\tau_2 = \infty$, [i.e., solving Equation (11) for f assuming $s = 0$] at each iteration yields

$$U_{i,j}^{k+1} = \Big(\mathbf{I} - \tau_1 \alpha_i \mathbf{A}\Big)^{-1} \Big[U_{i,j}^{k} + \tau_1 \mathbf{H}^T [\mathbf{H}\mathbf{S}_i^k F^k - Y_i] \cdot \partial_j \, \mathbf{S}_i^k F^k\Big],$$

$$F^{k+1} = \Big(-\beta\mathbf{A} + \sum_{i=1}^{m} (\mathbf{S}_i^{k+1})^T \mathbf{H}^T \mathbf{H} \mathbf{S}_i^{k+1}\Big)^{-1} \Big[\sum_{i=1}^{m} (\mathbf{S}_i^{k+1})^T \mathbf{H}^T Y_i\Big],$$

with initialization vectors $F^0 = U_{i,j}^0 = 0_{\mathbb{R}^{n^d}}$, for $i = 1, \ldots, m$, $j = 1, \ldots, d$.

6 Concluding Remarks

Accurate motion estimation is a fundamental challenge of the super-resolution problem. Some recent promising advances in this area have been focused on

coupling or combing the super-resolution reconstruction and the motion estimation. However, the existing approach is limited to parametric motion models, e.g., affine [4]. In this paper, we addressed the coupled super-resolution problem with a *non-parametric* motion model. We addressed the problem in a variational formulation and proposed a PDE-approach to yield a numerical scheme. In this approach, we used diffusion regularizations for both the motion and the super-resolved image. However, the approach is flexible and other suitable regularization schemes (e.g., total variation) may be employed in the proposed formulation. Furthermore, multi-scale implementations of the approach seem feasible and can improve the convergence of the numerical scheme towards a global minimizer. Finally, computational validation on other image sequences and addressing the problem of automatic parameter selection are natural steps in extending the presented theory.

Acknowledgements

This research was supported in part by the Natural Sciences and Engineering Research Council of Canada (NSERC) in the form of a Post-Doctoral Fellowship for Mehran Ebrahimi. This work was also supported by the Terry Fox Foundation for Cancer Research. The authors would like to thank Dr. Peter Burns and Ross Williams of the Sunnybrook Health Sciences Centre for providing the ultrasound data.

References

1. Aizawa, K., Komatsu, T., Saito, T.: Acquisition of very high-resolution images using stereo cameras. In: Proceedings of SPIE Visual Communications and Image Processing, Boston, MA, November 1991, vol. 1605, pp. 318–328 (1991)
2. Borman, S.: Topics in Multiframe Superresolution Restoration. PhD thesis, Graduate Program in Electrical Engineering, University of Notre Dame, Indiana (April 2004)
3. Chaudhuri, S.: Super-Resolution Imaging. Kluwer, Boston (2001)
4. Chung, J., Haber, E., Nagy, J.: Numerical methods for coupled super-resolution. Inverse Problems 22, 1261–1272 (2006)
5. Ebrahimi, M.: Inverse Problems and Self-Similarity in Imaging. PhD thesis, University of Waterloo (2008)
6. Ebrahimi, M., Vrscay, E.R.: Multi-frame super-resolution with no explicit motion estimation. In: Proceedings of The 2008 International Conference on Image Processing, Computer Vision, and Pattern Recognition, IPCV, Las Vegas, Nevada, USA, pp. 455–459 (2008)
7. Elad, M., Feuer, A.: Restoration of a single superresolution image from several blurred, noisy, and undersampled measured images. IEEE Transactions on Image Processing 6(12), 1646–1658 (1997)
8. Farsiu, S., Robinson, D., Elad, M., Milanfar, P.: Advances and challenges in super-resolution. International Journal of Imaging Systems and Technology 14(2), 47–57 (2004)

9. Farsiu, S., Robinson, D., Elad, M., Milanfar, P.: Fast and robust multi-frame super-resolution. IEEE Transactions on Image Processing 13(10), 1327–1344 (2004)
10. Fischer, B., Modersitzki, J.: Fast image registration: a variational approach. Applied Numerical Analysis and Computational Mathematics 1(1-2), A69–A74 (2004); (NACoM-2003), Cambridge, UK., May 23-26, vol. 1, pp. A69–A74. Wiley-VCH, Germany (2004)
11. Fischer, B., Modersitzki, J.: Ill-posed medicine-an introduction to image registration. Inverse Problems 24(3), 034008, 16 (2008)
12. Hardie, R., Barnard, K., Armstrong, E.: Joint MAP registration and high-resolution image estimation using a sequence of undersampled images. IEEE Transactions on Image Processing 6(12), 1621–1633 (1997)
13. Horn, B.K.P., Schunck, B.G.: Determining optical flow. Artificial Intelligence 17(1-3), 185–203 (1981)
14. Irani, M., Peleg, S.: Improving resolution by image registration. CVGIP: Graphical Model and Image Processing 53, 324–335 (1993)
15. Modersitzki, J.: Numerical methods for image registration. Oxford University Press, Oxford (2004)
16. Nguyen, N.X.: Numerical Algorithms for Image Superresolution. PhD thesis, Graduate Program in Scientific Computation and Computational Mathematics, Stanford University (July 2000)
17. Papoulis, A.: Generalized sampling expansion. IEEE Transactions on Circuits and Systems 24, 652–654 (1997)
18. Sauer, K., Allebach, J.: Iterative reconstruction of band-limited images from non-uniformly spaced samples. IEEE Transactions on Circuits and Systems, 1497–1505 (1987)
19. Schoenemann, T., Cremers, D.: High resolution motion layer decomposition using dual-space graph cuts. In: CVPR. IEEE Computer Society, Los Alamitos (2008)
20. Schultz, R., Stevenson, R.: Extraction of high-resolution frames from video sequences. IEEE Transactions on Image Processing 5, 996–1011 (1996)
21. Shannon, C.E.: Communication in the presence of noise. Proceedings of the IRE 37, 10–21 (1949)
22. Shekarforoush, H., Chellappa, R.: Data-driven multi-channel super-resolution with application to video sequences. Journal of the Optical Society of America A 16(3), 481–492 (1999)
23. Tekalp, A., Ozkan, M., Sezan, M.: High-resolution image econstruction from lower-resolution image sequences and space-varying image restoration. In: Proceedings of the IEEE International Conference on Acoustics, Speech and Signal Processing, San Francisco, CA, vol. 3, pp. 169–172 (1992)
24. Thirion, J.P.: Fast non-rigid matching of 3d medical images. In: Medical Robotics and Computer Aided Surgery (MRCAS), Baltimore, pp. 47–54 (1995)
25. Thirion, J.P.: Image matching as a diffusion process: an analogy with maxwell's demons. Medical Image Analysis 2(3), 243–260 (1998)
26. Tsai, R., Huang, T.: Multi-frame image restoration and registration. In: Advances in Computer Vision and Image Processing, Greenwich, CT, vol. 1 (1984)
27. Ur, H., Gross, D.: Improved resolution from subpixel shifted pictures. CVGIP: Graphical Models and Image Processing 54(2), 181–186 (1992)

Appendix 1: Proof of Theorem 1

Proof. Split the variation $v(x)$ as $v(x) := \big(v_1(x), \dots, v_m(x), g(x)\big)$ in which $v_i(x) \in \mathbb{R}^d$, $i = 1, \dots, m$ and $g(x) \in \mathbb{R}$. Also define,

$$p_i(x) := \mathcal{H}^*[\mathcal{H}\mathcal{S}_i f(x) - y_i(x)]\nabla \mathcal{S}_i f(x), \quad i = 1, \dots, m,$$
$$q(x) := -\sum_{i=1}^{m} \mathcal{S}_i^* \mathcal{H}^*[\mathcal{H}\mathcal{S}_i f(x) - y_i(x)].$$

Using the Taylor expansion of $f_{u_i+hv_i}(x)$ and $g_{u_i+hv_i}(x)$ with respect to h at the point $x - u(x)$,

$$f_{u_i+hv_i}(x) = f(x - u_i(x) - hv_i(x))) = f_{u_i}(x) - h\langle \nabla f_{u_i}(x), v_i(x)\rangle_{\mathbb{R}^d} + \mathcal{O}(h^2),$$

$$g_{u_i+hv_i}(x) = g(x - u_i(x) - hv_i(x))) = g_{u_i}(x) - h\langle \nabla g_{u_i}(x), v_i(x)\rangle_{\mathbb{R}^d} + \mathcal{O}(h^2),$$

for every $i = 1, \dots, m$. Directly using the definitions and the linearity of $\mathcal{H}$

$$\begin{aligned}
&d\ \mathcal{C}\ [y;(u,f);v] \\
&= \lim_{h\to 0} \frac{1}{h}(\mathcal{C}[y;(u,f)+hv] - \mathcal{C}[y;(u,f)]) \\
&= \lim_{h\to 0} \frac{1}{h}(\mathcal{C}[y;(u_1+hv_1,\dots,u_m+hv_m,f+hg)] - \mathcal{C}[y;(u_1,\dots,u_m,f)]) \\
&= \lim_{h\to 0} \frac{1}{2h} \sum_{i=1}^{m} \int_\Omega [y_i(x) - \mathcal{H}(f+hg)_{u_i+hv_i}(x)]^2 - [y_i(x) - \mathcal{H}f_{u_i}(x)]^2\ dx \\
&= \lim_{h\to 0} \frac{1}{2h} \sum_{i=1}^{m} \int_\Omega [y_i(x) - \mathcal{H}f_{u_i+hv_i}(x) - h\mathcal{H}g_{u_i+hv_i}(x)]^2 - [y_i(x) - \mathcal{H}f_{u_i}(x)]^2\ dx \\
&= \lim_{h\to 0} \frac{1}{2h} \sum_{i=1}^{m} \int_\Omega [y_i(x) - \mathcal{H}(f_{u_i}(x) - h\langle \nabla f_{u_i}(x), p(x)\rangle_{\mathbb{R}^d} + \mathcal{O}(h^2)) - h\mathcal{H}g_{u_i}(x) + \mathcal{O}(h^2)]^2 \\
&- [y_i(x) - \mathcal{H}f_{u_i}(x)]^2\ dx \\
&= \lim_{h\to 0} \frac{1}{2h} \sum_{i=1}^{m} \int_\Omega 2[y_i(x) - \mathcal{H}f_{u_i}(x)][h]\mathcal{H}(\langle \nabla f_{u_i}(x), v_i(x)\rangle_{\mathbb{R}^d} - g_{u_i}(x)) + \mathcal{O}(h^2)dx \\
&= -\sum_{i=1}^{m} \int_\Omega [\mathcal{H}f_{u_i}(x) - y_i(x)]\mathcal{H}(\langle \nabla f_{u_i}(x), v_i(x)\rangle_{\mathbb{R}^d} - g_{u_i}(x))dx \\
&= -\sum_{i=1}^{m} \int_\Omega \Big[[\mathcal{H}f_{u_i}(x) - y_i(x)]\mathcal{H}(\langle \nabla f_{u_i}(x), v_i(x)\rangle_{\mathbb{R}^d})\Big]dx + \sum_{i=1}^{m} \int_\Omega [\mathcal{H}f_{u_i}(x) - y_i(x)]\mathcal{H}g_{u_i}(x)dx.
\end{aligned}$$

Hence,

$$
\begin{aligned}
& d\ \mathcal{C}\ [y;(u,f);v] \\
&= -\sum_{i=1}^{m} \left\langle [\mathcal{H}f_{u_i}(x) - y_i(x)], \mathcal{H}(\langle \nabla f_{u_i}(x), v_i(x)\rangle_{\mathbb{R}^d}) \right\rangle_{\mathcal{L}^2(\Omega)} \\
&\quad + \sum_{i=1}^{m} \left\langle [\mathcal{H}f_{u_i}(x) - y_i(x)], \mathcal{H}g_{u_i}(x) \right\rangle_{\mathcal{L}^2(\Omega)} \\
&= -\sum_{i=1}^{m} \left\langle \mathcal{H}^*[\mathcal{H}f_{u_i}(x) - y_i(x)], (\langle \nabla f_{u_i}(x), v_i(x)\rangle_{\mathbb{R}^d}) \right\rangle_{\mathcal{L}^2(\Omega)} \\
&\quad + \sum_{i=1}^{m} \left\langle \mathcal{H}^*[\mathcal{H}f_{u_i}(x) - y_i(x)], g_{u_i}(x) \right\rangle_{\mathcal{L}^2(\Omega)} \\
&= -\sum_{i=1}^{m} \left\langle \mathcal{H}^*[\mathcal{H}f_{u_i}(x) - y_i(x)], (\langle \nabla f_{u_i}(x), v_i(x)\rangle_{\mathbb{R}^d}) \right\rangle_{\mathcal{L}^2(\Omega)} \\
&\quad + \sum_{i=1}^{m} \left\langle \mathcal{H}^*[\mathcal{H}f_{u_i}(x) - y_i(x)], \mathcal{S}_i g(x) \right\rangle_{\mathcal{L}^2(\Omega)} \\
&= -\sum_{i=1}^{m} \left\langle \mathcal{H}^*[\mathcal{H}f_{u_i}(x) - y_i(x)], (\langle \nabla f_{u_i}(x), v_i(x)\rangle_{\mathbb{R}^d}) \right\rangle_{\mathcal{L}^2(\Omega)} \\
&\quad + \sum_{i=1}^{m} \left\langle \mathcal{S}_i^*\mathcal{H}^*[\mathcal{H}f_{u_i}(x) - y_i(x)], g(x) \right\rangle_{\mathcal{L}^2(\Omega)} \\
&= -\sum_{i=1}^{m} \int_\Omega \langle p_i(x), v_i(x)\rangle_{\mathbb{R}^d}\ dx + \sum_{i=1}^{m} \int_\Omega \mathcal{S}_i^*\mathcal{H}^*[\mathcal{H}f_{u_i}(x) - y_i(x)]g(x)\ dx \\
&= -\int_\Omega \left[\sum_{i=1}^{m} \langle p_i(x), v_i(x)\rangle_{\mathbb{R}^d} - \sum_{i=1}^{m} \mathcal{S}_i^*\mathcal{H}^*[\mathcal{H}f_{u_i}(x) - y_i(x)]g(x) \right] dx \\
&= -\int_\Omega \left[\sum_{i=1}^{m} \langle p_i(x), v_i(x)\rangle_{\mathbb{R}^d} + q(x)g(x) \right] dx \\
&= -\int_\Omega \langle p_1(x), v_1(x)\rangle_{\mathbb{R}^d} + \cdots + \langle p_m(x), v_m(x)\rangle_{\mathbb{R}^d} + \langle q(x), g(x)\rangle_{\mathbb{R}} \Big] dx \\
&= -\int_\Omega \left\langle \Big(p_1(x), \ldots, p_m(x), q(x)\Big), \Big(v_1(x), \ldots, v_m(x), g(x)\Big) \right\rangle_{\mathbb{R}^{md+1}} dx \\
&= -\int_\Omega \langle \Phi(x, u(x), f(x)), v(x)\rangle_{\mathbb{R}^{md+1}}\ dx.
\end{aligned}
$$

Appendix 2: Definition of A

$\mathbf{A} \in \mathbb{R}^{n^d \times n^d}$ is defined as $\mathbf{A} := \sum_{l=1}^{d} \mathbf{A}_l$ where $\mathbf{A}_l = \underbrace{\mathbf{I} \otimes \cdots \otimes \mathbf{I}}_{l-1 \text{ times}} \otimes \mathbf{B} \otimes \underbrace{\mathbf{I} \otimes \cdots \otimes \mathbf{I}}_{d-l \text{ times}}$, in which $\mathbf{I} \in \mathbb{R}^{n \times n}$ is identity matrix and $\otimes$ denotes the Kronecker product of matrices. The l^{th} factor $\mathbf{B} \in \mathbb{R}^{n \times n}$ is an approximation of the second order derivative in only one spatial direction. More precisely, it can be defined as the tridiagonal matrix

$$\mathbf{B} = \begin{pmatrix} -2 & 1 & 0 & \dots & 0 \\ 1 & -2 & 1 & \dots & 0 \\ \vdots & \ddots & \ddots & \ddots & \vdots \\ 0 & \dots & 1 & -2 & 1 \\ 0 & \dots\dots & 1 & -2 \end{pmatrix}.$$

Appendix 3: Construction of Matrices K, D, and H

Given the zooming factor $z \in \mathbb{N}$, we define $\mathbf{K} \in \mathbb{R}^{(n-z+1)^d \times n^d}$ as $\mathbf{K} := \underbrace{\mathbf{K}_1 \otimes \cdots \otimes \mathbf{K}_1}_{d \text{ times}}$ in which $\mathbf{K}_1 \in \mathbb{R}^{(n-z+1) \times n}$ is

$$\mathbf{K}_1 = \frac{1}{z} \begin{pmatrix} \underbrace{1 \dots 1}_{z \text{ times}} \underbrace{0 \dots\dots\dots\dots\dots 0}_{n-z \text{ times}} \\ 0 \underbrace{1 \dots 1}_{z \text{ times}} \underbrace{0 \dots\dots\dots\dots 0}_{n-z-1 \text{ times}} \\ 0\ 0 \underbrace{1 \dots 1}_{z \text{ times}} \underbrace{0 \dots\dots\dots 0}_{n-z-2 \text{ times}} \\ \vdots \quad \vdots \quad \vdots \quad \vdots \\ \underbrace{0 \dots\dots\dots\dots\dots 0}_{n-z \text{ times}} \underbrace{1 \dots 1}_{z \text{ times}} \end{pmatrix}.$$

Also, $\mathbf{D} \in \mathbb{R}^{\lfloor n/z \rfloor^d \times (n-z+1)^d}$ is defined as $\mathbf{D} := \underbrace{\mathbf{D}_1 \otimes \cdots \otimes \mathbf{D}_1}_{d \text{ times}}$, where $\mathbf{D}_1 \in \mathbb{R}^{\lfloor n/z \rfloor \times (n-z+1)}$ is

$$\mathbf{D}_1 = \begin{pmatrix} 1 & \underbrace{0 \dots\dots\dots\dots\dots\dots\dots\dots\dots 0}_{n-z \text{ times}} \\ \underbrace{0 \dots\dots 0}_{z \text{ times}} & 1 & \underbrace{0 \dots\dots\dots\dots\dots\dots\dots 0}_{n-2z \text{ times}} \\ \underbrace{0 \dots\dots\dots\dots 0}_{2z \text{ times}} & 1 & \underbrace{0 \dots\dots\dots\dots\dots 0}_{n-3z} \\ & \vdots \quad \vdots \quad \vdots \quad \vdots \\ \underbrace{0 \dots\dots\dots\dots\dots\dots\dots 0}_{(\lfloor n/z \rfloor - 1)z \text{ times}} & 1 & \underbrace{0 \dots\dots 0}_{n-(\lfloor n/z \rfloor)z \text{ times}} \end{pmatrix}.$$

Finally, $\mathbf{H} \in \mathbb{R}^{\lfloor n/z \rfloor^d \times n^d}$ is defined as the matrix multiplication of $\mathbf{H} := \mathbf{D} \times \mathbf{K}$.